


Article

Electrochemical Oxidation of Sodium Metabisulfite for Sensing Zinc Oxide Nanoparticles Deposited on Graphite Electrode

Kailai Wang and Edward P. C. Lai * 

Department of Chemistry, Ottawa-Carleton Chemistry Institute, Carleton University, Ottawa, ON K1S 5B6, Canada; kailaiwang@cmail.carleton.ca

* Correspondence: edward.lai@carleton.ca; Tel.: +1-(613)-520-2600 (ext. 3835); Fax: +1-(613)-520-3749

Abstract: A novel concept was successfully evaluated for the electrochemical quantitative analysis of zinc oxide nanoparticles originally in aqueous suspension. An aliquot of the suspension was first placed on the working area of a graphite screen-printed electrode and the water was evaporated to form a dry deposit of ZnO nanoparticles. Deposition of ZnO nanoparticles on the electrode was confirmed by energy-dispersive X-ray spectroscopy. A probe solution containing KCl and sodium metabisulfite was added on top of the deposit for electrochemical analysis by cyclic voltammetry. The anodic peak current (I_{pa}) for metabisulfite, measured at +1.2 V vs. Ag/AgCl, afforded a lower detection limit of 3 μg and exhibited a linear dependence on the mass of deposited ZnO nanoparticles up to 15 μg . Further, the current increased nonlinearly until it reached a saturation level beyond 60 μg of ZnO nanoparticles. The diffusion coefficient of metabisulfite anions through the electrical double layer was determined to be $4.16 \times 10^{-5} \text{ cm}^2/\text{s}$. Apparently the surface reactivity of ZnO originated from the oxide anion rather than the superoxide anion or the hydroxyl radical. Enhancement of the metabisulfite oxidation peak current can be developed into a sensitive method for the quantitation of ZnO nanoparticles.

Keywords: cyclic voltammetry; electrochemical analysis; nanoparticles; sodium metabisulfite; surface reactivity; zinc oxide



Citation: Wang, K.; Lai, E.P.C. Electrochemical Oxidation of Sodium Metabisulfite for Sensing Zinc Oxide Nanoparticles Deposited on Graphite Electrode. *Chemosensors* **2022**, *10*, 145. <https://doi.org/10.3390/chemosensors10040145>

Academic Editor: Alexey Glushenkov

Received: 8 March 2022

Accepted: 11 April 2022

Published: 13 April 2022

Publisher's Note: MDPI stays neutral with regard to jurisdictional claims in published maps and institutional affiliations.



Copyright: © 2022 by the authors. Licensee MDPI, Basel, Switzerland. This article is an open access article distributed under the terms and conditions of the Creative Commons Attribution (CC BY) license (<https://creativecommons.org/licenses/by/4.0/>).

1. Introduction

Transition metal oxide nanoparticles are produced in large quantities for the manufacturing of many consumer and industrial goods. The band gap and electronic structure of these oxides can be controlled by their nanoparticle size, resulting in wide applications for microelectronics, energy storage, and electrochemical sensors due to their tunable chemical and physical properties [1,2]. Among transition metals, zinc oxide (ZnO) nanoparticles are applied in a variety of antibacterial materials, biosensors, catalysts, paints, personal care products, pharmaceuticals, photodynamic therapy, sunscreens and supercapacitors [3–11]. ZnO also exhibits high charge carrier mobilities for solar water splitting [12] and can be an active catalyst for water oxidation reaction to generate H_2O_2 [13]. Applications of ZnO extend to photoelectrochemical water splitting and microwave absorption, considering its photoactivity and dielectric properties [14,15]. Irradiation of ZnO aqueous suspension by UV light enhances the photocatalytic generation of hydroxyl radicals in water [16,17]. Interestingly, ZnO can be reduced within the nanoparticles when in direct contact with an electrode [18]. As an alternative to chemical preparation, green synthesis and physical methods [19,20], microorganisms have recently emerged in the biosynthesis of ZnO nanoparticles due to their low cost and ecofriendly nature [21]. A previous assay using 1,1-diphenyl-2-picrylhydrazyl (DPPH) indicated that ZnO nanoparticles have oxidant activity with an IC_{50} value of 128 $\mu\text{g}/\text{mL}$ [22]. These nanoparticles can produce reactive oxygen species (ROS), and the oxidation capacity towards γ -L-glutamyl-L-cysteinyl-glycine (GSH) oxidation stress accounts for their antimicrobial behavior [23]. The toxicity of ZnO

nanoparticles may be attributed to their dissolution in water to produce Zn^{2+} ions. The generation of ROS causes oxidative stress in biological cells and induces cytotoxicity in cancer cells [24], depending on their size and shape [25–27]. The accumulation of ZnO nanoparticles in biological cells can alter cellular membranes [28] and bring about undesirable antitumor activity [29].

Zinc oxide is an essential chemical in the rubber and pharmaceutical industries. At the nanoscale, zinc oxide has shown antimicrobial properties which make it potentially excellent for application to water disinfection [30]. Due to the toxicity of ZnO nanoparticles to environmental organisms, the development of analytical methods that can determine the residual concentration of ZnO nanoparticles in water samples after membrane filtration is needed to meet the increasing demand. Several instrumental methods of analysis are found to be useful for the quantitation of nanoparticles, including single particle inductively coupled plasma mass spectrometry (SP-ICP-MS) [31], cloud point extraction ICP-MS [32], energy dispersive X-ray spectroscopy [33,34], electrochemical impedance spectroscopy [35–37], nonlinear optical spectroscopy, transmission electron microscopy (TEM) and UV-visible absorption spectroscopy [38]. Electrochemical analysis can detect and quantify nanoparticles, based on the measurement of Faradaic charge transfer when nanoparticles were reduced or oxidized by a microelectrode [39]. Cyclic voltammetry (CV) is a major electrochemical technique that is commonly used for analyzing redox chemistry in industrial and research settings. It has recently been applied to investigate the antioxidant activity of polyphenols in wine [40] and assess the antioxidant capacity of biological samples [41] that was traditionally measured by enzymatic biochemical and biological tests [42].

Sodium metabisulfite ($Na_2S_2O_5$) is an inorganic salt of sulfurous acid that dissolves in water to form sodium, bisulfite and sulfite ions: $Na_2S_2O_5 + H_2O = 2Na^+ + 2HSO_3^-$ and $HSO_3^- = H^+ + SO_3^{2-}$ [43]. When oxygen is present, bisulfite anions are converted to sulfate anions: $2HSO_3^- + O_2 = 2H^+ + 2SO_4^{2-}$. The salt is commonly used as an antioxidant agent in a variety of pharmaceutical formulations and dental base materials [44–46], cosmetics and personal care products [47,48], cookies and crackers [49], reverse osmosis systems [50], food packaging films [51] and aluminum alloys [52]. A glassy carbon electrode was modified with a porphyrin complex film for the analysis of sodium metabisulfite in pharmaceuticals. A unique anodic peak at 0.5 V was attributed to the oxidation of sulfite to sulfate [53]. The influence of metabisulfite on the platinum electrode had previously been analyzed by CV. An anodic peak was observed in the region -0.6 V to -0.3 V vs. SCE in the anodic potential direction and a corresponding cathodic peak in the region -0.5 V to -0.8 V when the scan was reverted in the cathodic direction. Those peaks could be ascribed to the hydrogen adsorption/desorption reactions [54]. Cyclic voltammetry, linear sweep voltammetry and differential pulse voltammetry were used to investigate the electrochemical performance of an Au/F-rGO sensor for the quantification of sodium metabisulfite [55]. In this research work, a new electrochemical method was developed to attain simple and cost-effective quantitative analysis of ZnO nanoparticles in aqueous suspension for environmental science and engineering applications. The general detection principle involves the pre-deposition of the ZnO nanoparticles from an aliquot (150 μ L) of water sample on a graphite screen printed electrode (SPE) by overnight evaporation at room temperature in a controlled environment. A test solution containing KCl and sodium metabisulfite was added on top of the deposit for analysis by CV. Sodium metabisulfite was used as a redox probe with unique electrochemical behavior for sensitivity enhancement in the quantitative analysis of ZnO nanoparticles. The anodic peak current (I_{pa}) for metabisulfite was measured at +1.2 V vs. Ag/AgCl to establish a linear relationship with the mass of deposited ZnO nanoparticles.

2. Materials and Method

2.1. Materials

Zinc oxide nanoparticles (<50 nm, >97%), sodium metabisulfite, potassium chloride, L-glutathione, potassium ferricyanide and ascorbic acid were purchased from Sigma-Aldrich (Oakville, ON, Canada).

2.2. Electrochemical Analysis

An electrochemical analyzer (Homiangz μ EA160C, Longman, CO, USA) was used for all electrochemical analysis by cyclic voltammetry (CV). Specific experimental parameters were: initial potential: 0.0 V, high potential: 1.4 V, low potential: 0.0 V, scan rate: 0.1 V/s, scan initial direction: positive, segments: 2, sample interval: 0.001 V, quiescent time: 2 s, and sensitivity: 10 mA. Measurements were carried out using Zensor TE100 screen printed electrodes (SPE) produced by EDAQ (Colorado Springs, CO, USA) with a graphitic working electrode, a graphitic auxiliary electrode, and an Ag/AgCl pellet reference electrode. Every aqueous suspension of ZnO nanoparticles was homogenized with an ultrasonic probe operating at 100 Watts for 1 min before CV analysis at 25 °C.

2.3. Sample Preparation

Standard aqueous suspensions of ZnO nanoparticles (22–860 μ g/mL) were freshly prepared to avoid suspension stability problems, by serial dilution of a stock with ultrasonic homogenization, before CV analysis [56]. An aliquot (150 μ L) was dispensed on each SPE and allowed to evaporate at room temperature overnight in a controlled environment. A solution of Na₂S₂O₅ (0.003 or 0.010 M), glutathione (0.003 M) or ascorbic acid (0.090 M) in KCl (1.0 M) was then added on top as the sample for CV analysis to measure the anodic oxidation peak current. Nanomaterials had previously been analyzed by CV in 1.0 M KCl solution [57,58].

2.4. Scanning Electron Microscopy

Scanning electron microscopy (SEM) imaging of SPEs, without and with a deposit of ZnO nanoparticles, was performed on a TESCAN Vega II XMU system (Brno, Czech Republic). An INCA X-Act detector (10 mm²) from Oxford Instruments (Bucks, UK) was attached for elemental analysis of the SPEs by energy dispersive X-ray (EDX) spectroscopy.

3. Results and Discussion

Oxidation of sodium metabisulfite directly by ZnO nanoparticles in aqueous suspension was tested first. As shown in Figure 1, the metabisulfite oxidation peak currents were observed to decrease with increasing ZnO nanoparticle concentrations up to 0.4 mg/mL. This steep downward trend indicates either adsorption of metabisulfite by the nanoparticles before CV analysis of each suspension. For nanoparticle concentrations above 0.4 mg/mL, the peak currents reverted to a gentle upward trend probably due to the agglomeration of ZnO nanoparticles and hence the reduction of available surface area for metabisulfite adsorption. The trend observed in the first test was confirmed by repeating the CV analysis with freshly prepared suspensions in the second test. The aggregation of spherical ZnO nanoparticles exhibits a strong dependence on the ionic strength of the solution; the critical coagulation concentration increases significantly as the pH goes away from the point of zero charge [59]. Due to various interactions between nanoparticles of different surface morphologies and size distributions, further experiments will be needed to gain further insight for a better understanding of the challenges with the quantitative analysis of nanoparticles in aqueous suspension.

The oxidation peak currents for metabisulfite were compared with those obtained for ascorbic acid, one of the standard antioxidants that are capable of terminating a chain oxidation reaction by eliminating free radical intermediates. They act as antioxidants by being oxidized, hence antioxidants can be considered as reducing agents [60]. However, unlike metabisulfite, the ascorbic acid oxidation peak currents did not change significantly

with increasing ZnO nanoparticle concentrations up to 0.75 mg/mL. These results suggest that ascorbic acid, albeit well known to be an antioxidant providing protection against oxidative stress-induced cellular damage by scavenging of ROS, does not react quickly with ZnO nanoparticles in an aqueous suspension during a contact time of 5 min.

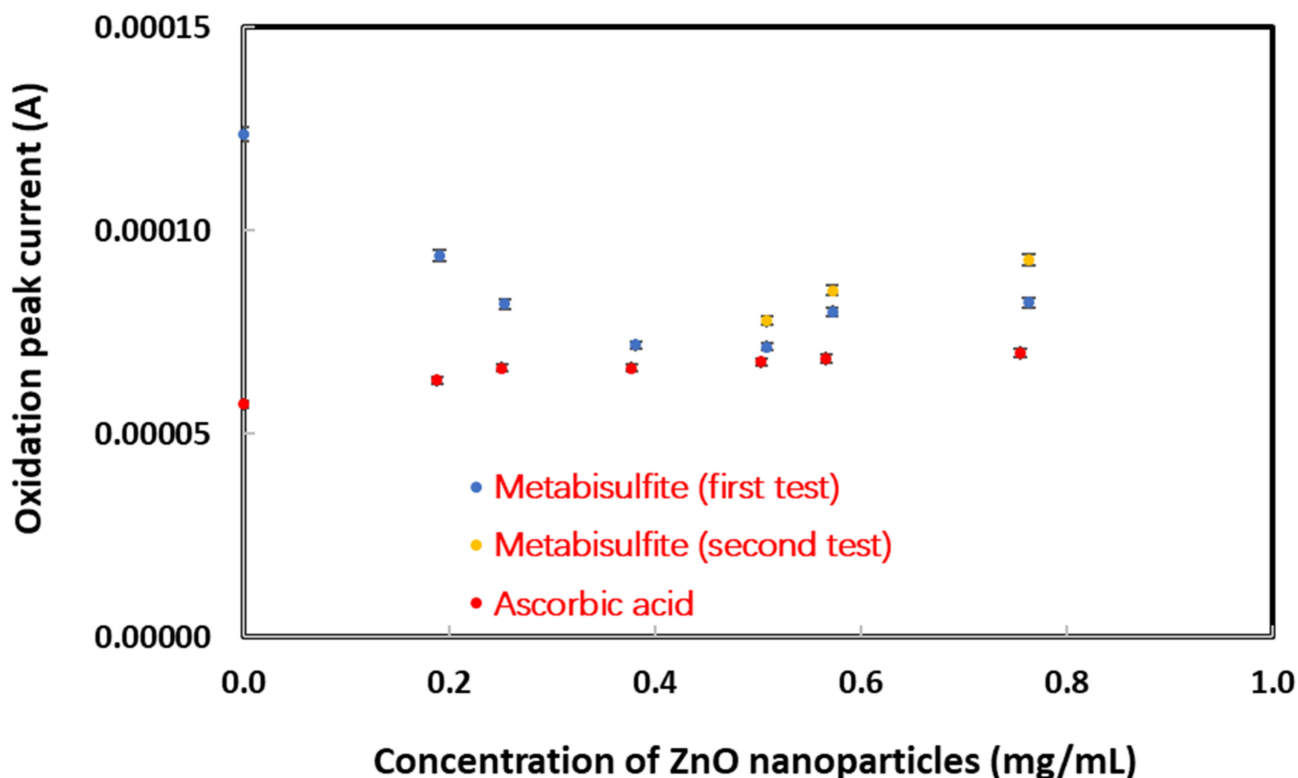


Figure 1. Cyclic voltammetric measurement results of metabisulfite and ascorbic acid (0.003 M in 1.0 M KCl) oxidation peak currents vs. concentration of ZnO nanoparticles dispersed in sample solution.

The difference in oxidation peak currents between ZnO nanoparticles in suspension and ZnO nanoparticles deposited on the SPE was studied by CV for metabisulfite and AA solutions. For sodium metabisulfite in Figure 2, its oxidation peak current obtained with ZnO deposited on the SPE was significantly higher than that obtained with ZnO suspended in the KCl electrolyte. On the contrary, Figure S1 (Supplementary Materials) shows that for a 0.003 M AA solution, the voltammograms obtained with ZnO in suspension and deposited on the SPE did not result in a big difference of oxidation peak currents (measured at their respective peak potentials).

The difference in oxidation peak currents between SPEs with and without ZnO nanoparticles (115 µg) deposited was also studied by CV. As shown in Figure S2, the ZnO deposit produced a strong oxidation peak current for metabisulfite at 1.2 V, with little overlap with the oxidation peak current of water molecules at 1.4 V. Energy dispersive X-ray spectroscopy (EDX) analysis in Figure 3 verifies the deposition of ZnO nanoparticles on the SPE, for comparison with a blank electrode that does not show any deposit of Zn nanoparticles.

Next, SPEs deposited with different amounts of ZnO nanoparticles were tested using potassium ferricyanide solution (0.006 M in 1.0 M KCl) as a negative control. The results in Figure S3 show nearly constant ferrocyanide oxidation peak currents (mean = 3.5×10^{-5} A) that did not increase with increasing amounts of deposited nanoparticles. As presented in Figure 4, the Zn element % by weight on each SPE measured by EDX verifies that there were ZnO nanoparticles deposited on all the SPEs to exhibit a direct proportional relationship. These two trends suggest that the electrode surface was fully covered by as

little as 13 μg of nanoparticles and more nanoparticles did not increase the effective surface area for ferrocyanide oxidation. Obviously, potassium ferricyanide cannot be used as a sensitive probe to facilitate CV detection or quantification of ZnO nanoparticles deposited by drying an unknown suspension on the SPE.

In stark contrast to potassium ferricyanide, sodium metabisulfite was demonstrated to be a sensitive probe for CV quantification of ZnO nanoparticles when a strong peak current (2.1×10^{-4} A) was obtained for 0.006 M sodium bisulfite. By measuring the HSO_3^- oxidation peak current from each first scan for different $\text{Na}_2\text{S}_2\text{O}_5$ concentrations, a linear relationship was observed between the two variables as shown in Figure S4. This finding suggested that any concentration of $\text{Na}_2\text{S}_2\text{O}_5$ within the range studied could provide a good probe and no optimization would be necessary except for the possible increase of analytical sensitivity. All SPEs had the same mass (either 60 μg or 115 μg) of ZnO nanoparticles deposited on the SPEs. These two masses were selected out of a broad range that would be required later to determine the linear dynamic range of this new method. Without ZnO nanoparticles, no oxidation peak was observed for metabisulfite. Interestingly, there was not much difference between the metabisulfite oxidation peak currents obtained with either mass of ZnO nanoparticles. One plausible explanation is that as the ZnO nanoparticles deposited on an SPE became larger than the monolayer amount, the SPE were fully covered by ZnO to give the maximum possible oxidation peak current.

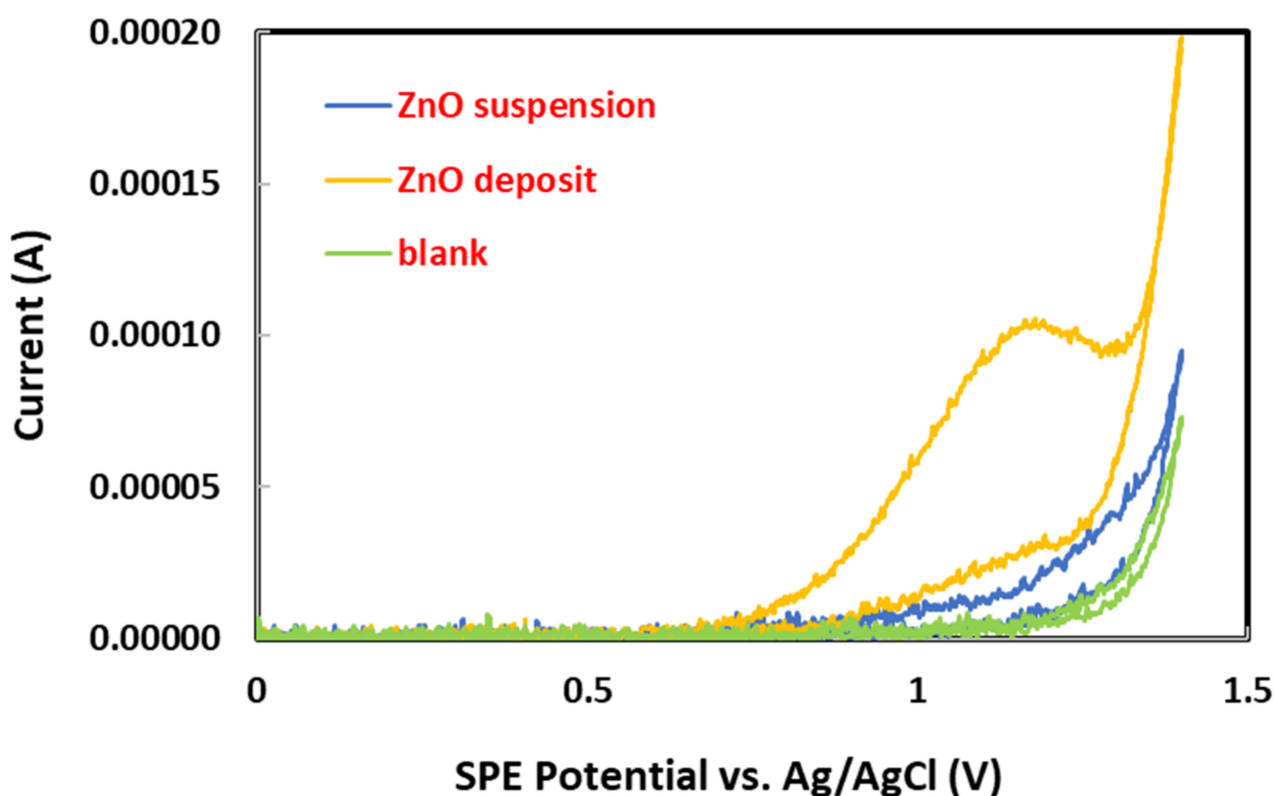


Figure 2. Cyclic voltammograms of sodium metabisulfite (0.003 M in 1.0 M KCl) on graphite electrode with ZnO nanoparticles in suspension (0.21 mg/mL) versus ZnO nanoparticles deposited on graphite electrode (150 μL of 0.21 mg/mL). $E_{\text{initial}} = 0.0$ V, $E_{\text{final}} = 1.4$ V, scan rate = 0.10 V/s, scan direction = positive.

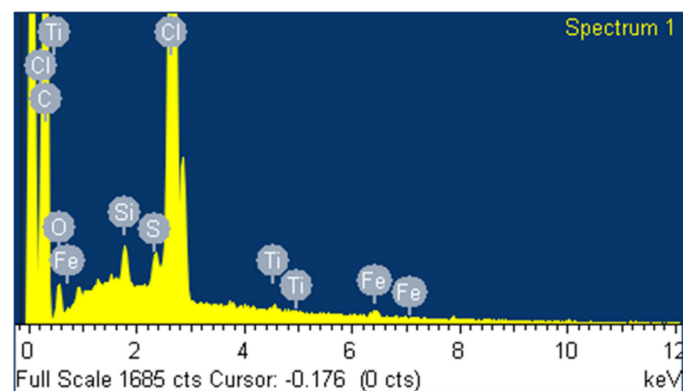
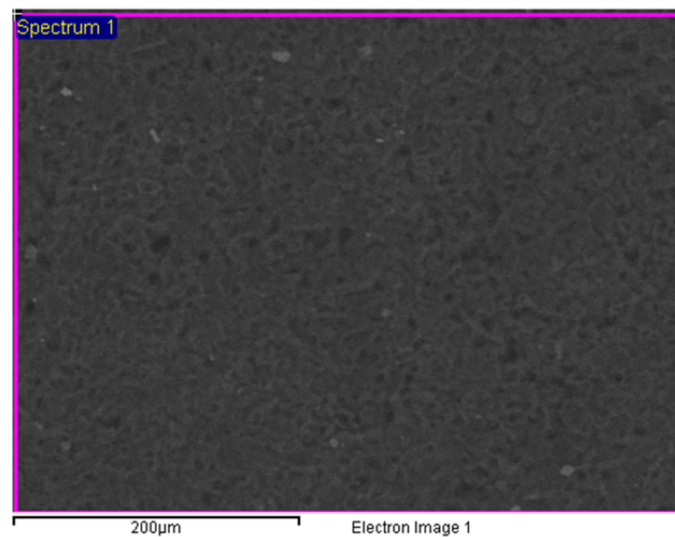
It has been shown above (in Figure 3) that a deposit of ZnO nanoparticles on the SPE produced a strong oxidation peak current for sodium metabisulfite. Further investigation revealed that, for any given metabisulfite concentration, there was a dependency between the oxidation peak current (measured at +1.2 V vs. Ag/AgCl) and the mass of ZnO nanoparticles deposited on SPE, as exemplified by 0.003 M and 0.01 M shown in Figure 5. A nearly

linear current response was attained from 3 μg up to 15 μg of ZnO nanoparticles for 0.01 M metabisulfite. The lower detection limit of 3 μg is adequate for wastewater treatment analysis. This novel electrochemical oxidation method is conceptually different from our previous work that was based on surface catalytic activity and charge storage capacity [61]. Larger amounts (than 15 μg) of nanoparticles continued to increase the oxidation current nonlinearly until it reached a saturated current level at 60 μg of ZnO and beyond. However, as ZnO is an insulator, the mechanistic process behind these enhancements of the metabisulfite oxidation peak current was not simply based on the increments of SPE surface area by the deposited ZnO nanoparticles. It might be related to the oxidation activity of ZnO nanoparticles as reported previously by Al-Mohaimed et al. [62].

Screen-printed graphite electrode

9/14/2021 2:41:36 PM

Element	Weight%	Atomic%
C K	107.48	92.00
O K	3.96	2.55
Si K	0.27	0.10
S K	0.23	0.07
Cl K	17.97	5.21
Ti K	0.09	0.02
Fe K	0.29	0.05
Totals	130.30	



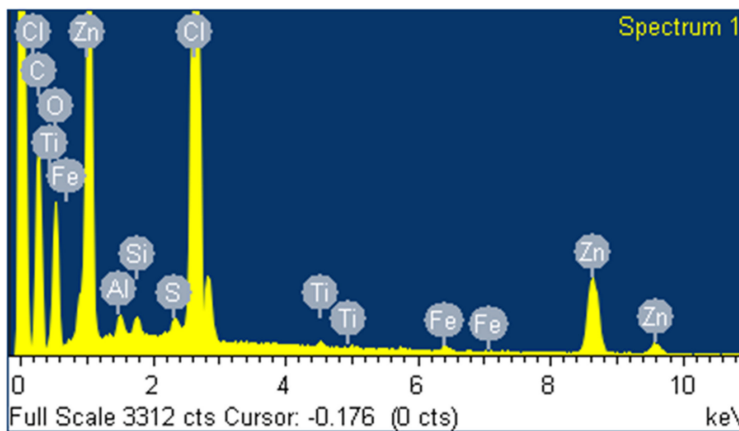
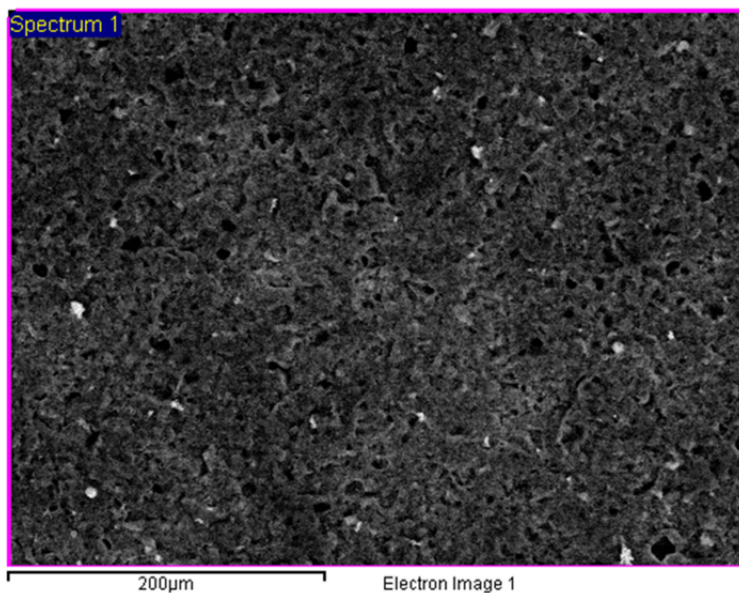
(a)

Figure 3. Cont.

Screen-printed graphite electrode with ZnO nanoparticles

9/14/2021 1:32:17 PM

Element	Weight%	Atomic%
C K	46.24	67.73
O K	18.83	20.70
Al K	0.35	0.23
Si K	0.30	0.19
S K	0.20	0.11
Cl K	14.71	7.30
Ti K	0.16	0.06
Fe K	0.31	0.10
Zn K	13.32	3.59
Totals	94.42	



(b)

Figure 3. Energy dispersive X-ray spectroscopy of (a) blank screen-printed electrode, and (b) screen-printed electrode with a deposit of ZnO nanoparticles.

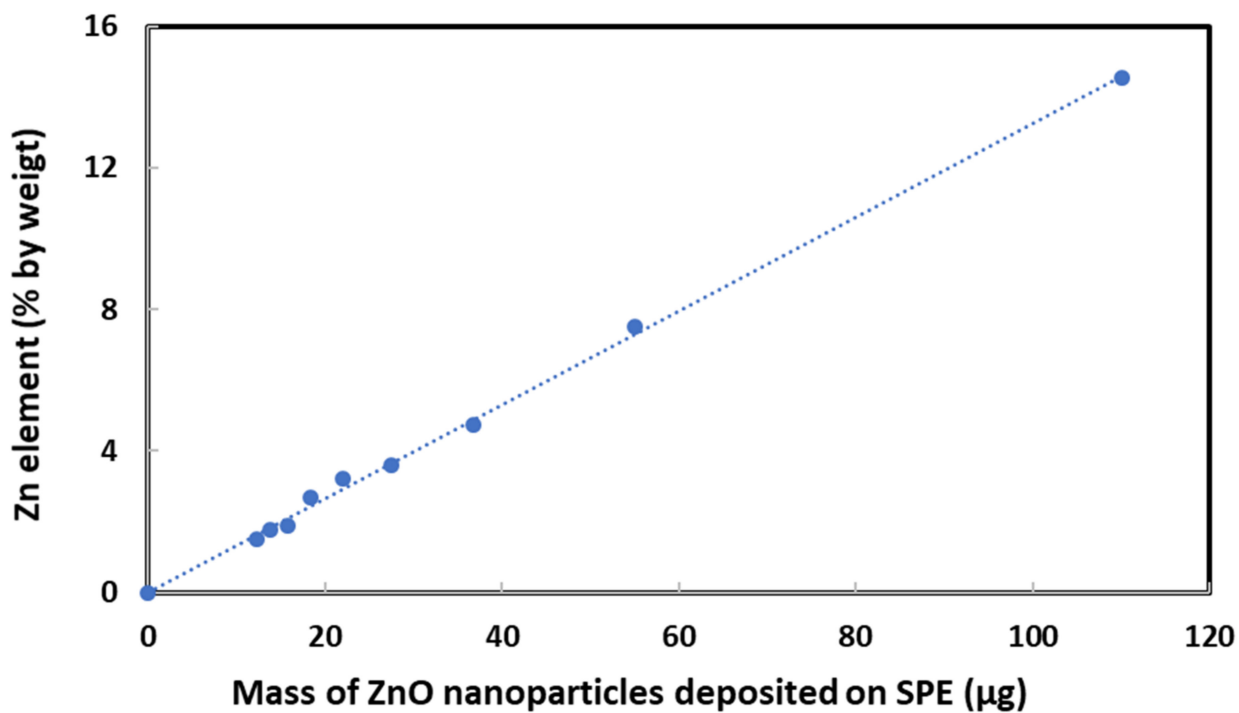


Figure 4. Energy dispersive X-ray analysis results of Zn element % by weight vs. mass of ZnO nanoparticles deposited on graphite electrode.

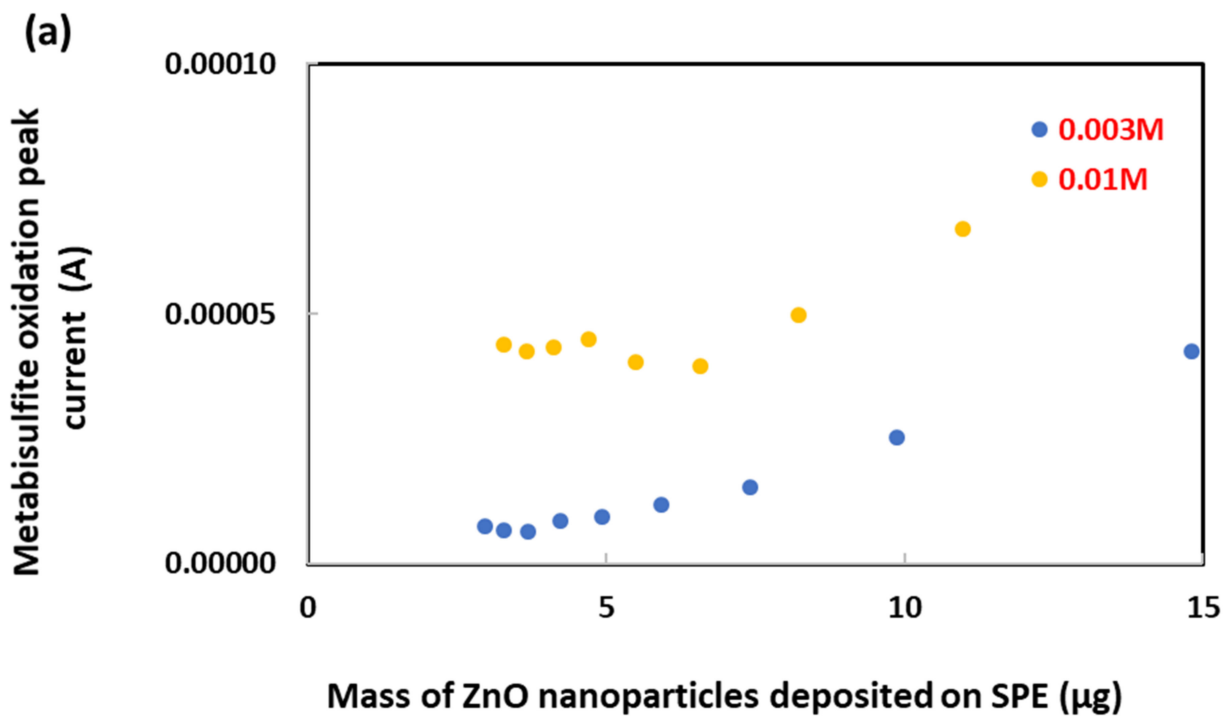


Figure 5. Cont.

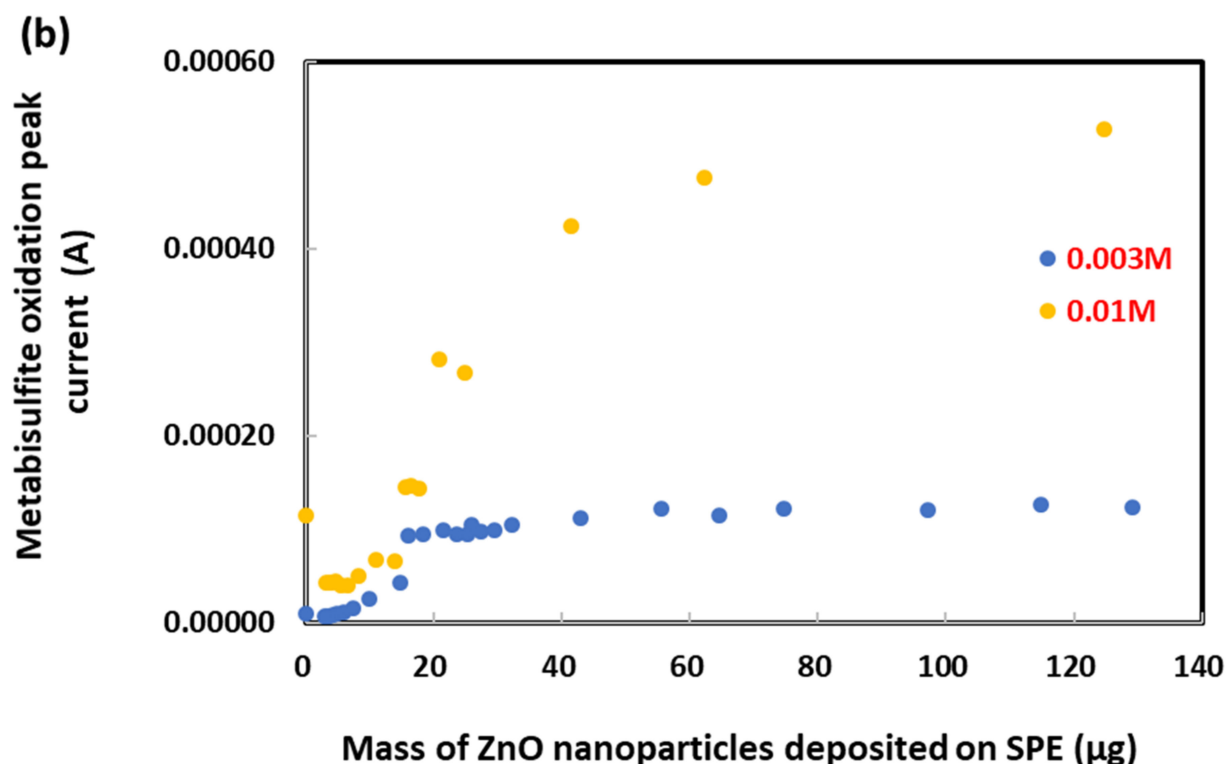
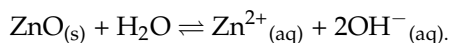


Figure 5. Cyclic voltammetric measurement results of sodium metabisulfite (0.003 M and 0.010 M in 1.0 M KCl) oxidation peak currents with (a) 0 to 15 µg and (b) 0 to 140 µg of ZnO nanoparticles deposited on graphite electrode.

Alternatively, the dissolution of ZnO nanoparticles produces free zinc ions and hydroxide ions [63]:



However, other than the Pourbaix diagram for ZnO [64], not much scientific literature can be found to explain how Zn^{2+} or OH^{-} could enhance the metabisulfite oxidation peak current. More research efforts will be needed to unravel the mechanistic process by studying other transition metal oxide nanoparticles.

The oxidation peak potential of sodium metabisulfite, as shown in Figures 6 and 7, seems to depend both on its concentration and the mass of ZnO nanoparticles deposited on the SPE, within a variation of ± 0.04 V. This dependency can probably be explained by the impact of sodium metabisulfite concentration on the ionic strength in each sample tested. Nevertheless, the obtained results for ZnO quantitative determination remained significant because they were based on the measurement of metabisulfite oxidation peak current.

Changes in the cyclic voltammograms acquired at different scan rates can be used as diagnostic criteria for the investigation of various electrochemical reaction mechanisms, even for processes with a complex stoichiometry [65]. The peak current I_p (A) measured in the forward potential scan, is given (for the case of reversible electron transfer) by the Randles–Sevcik equation: $I_p = (2.69 \times 10^5)n^{3/2}AD^{1/2}C\nu^{1/2}$, where n is the number of transferring electrons, A is the surface area of the graphite electrode (cm^2), D is the diffusion coefficient ($\text{cm}^2 \text{s}^{-1}$), C is the bulk concentration ($\text{mol}\cdot\text{cm}^{-3}$), and ν is the potential scan rate ($\text{V}\cdot\text{s}^{-1}$). We obtained information regarding the nature of the metabisulfite electrode process (if it is diffusion or adsorption controlled) by measuring the anodic peak current (I_{pa}) at different potential scan rates (ν) from 0.006 to 0.150 V/s. As shown in Figure 8a, a correlation coefficient of 0.9888 shows that the electron transfer was fast enough to maintain the equilibrium ratio between the reduced and the oxidized forms of the redox couple [66]. In Figure 8b, the logarithmic representation of $\ln(I_{pa})$ versus $\ln(\nu)$ generates

a slope parameter that indicates whether the electrode process is diffusion or adsorption controlled. Indeed, the slope result of 0.5504 indicates a diffusion-controlled process for the oxidation of metabisulfite rather than one being controlled by adsorption.

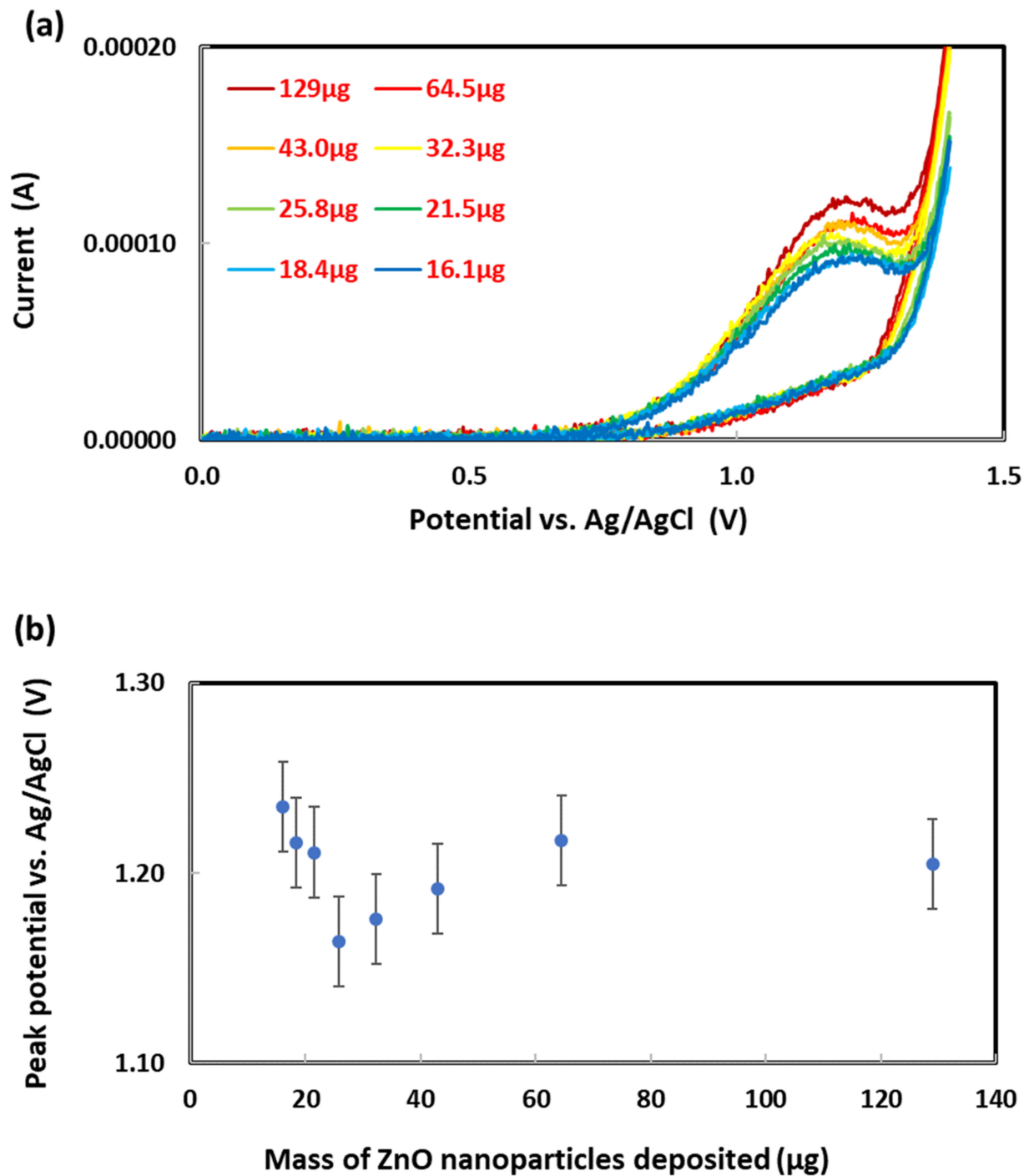


Figure 6. (a) Cyclic voltammograms of 0.003 M sodium metabisulfite on graphite electrodes deposited with different masses of ZnO nanoparticles. (b) Metabisulfite oxidation peak potential vs. mass of ZnO nanoparticles deposited.

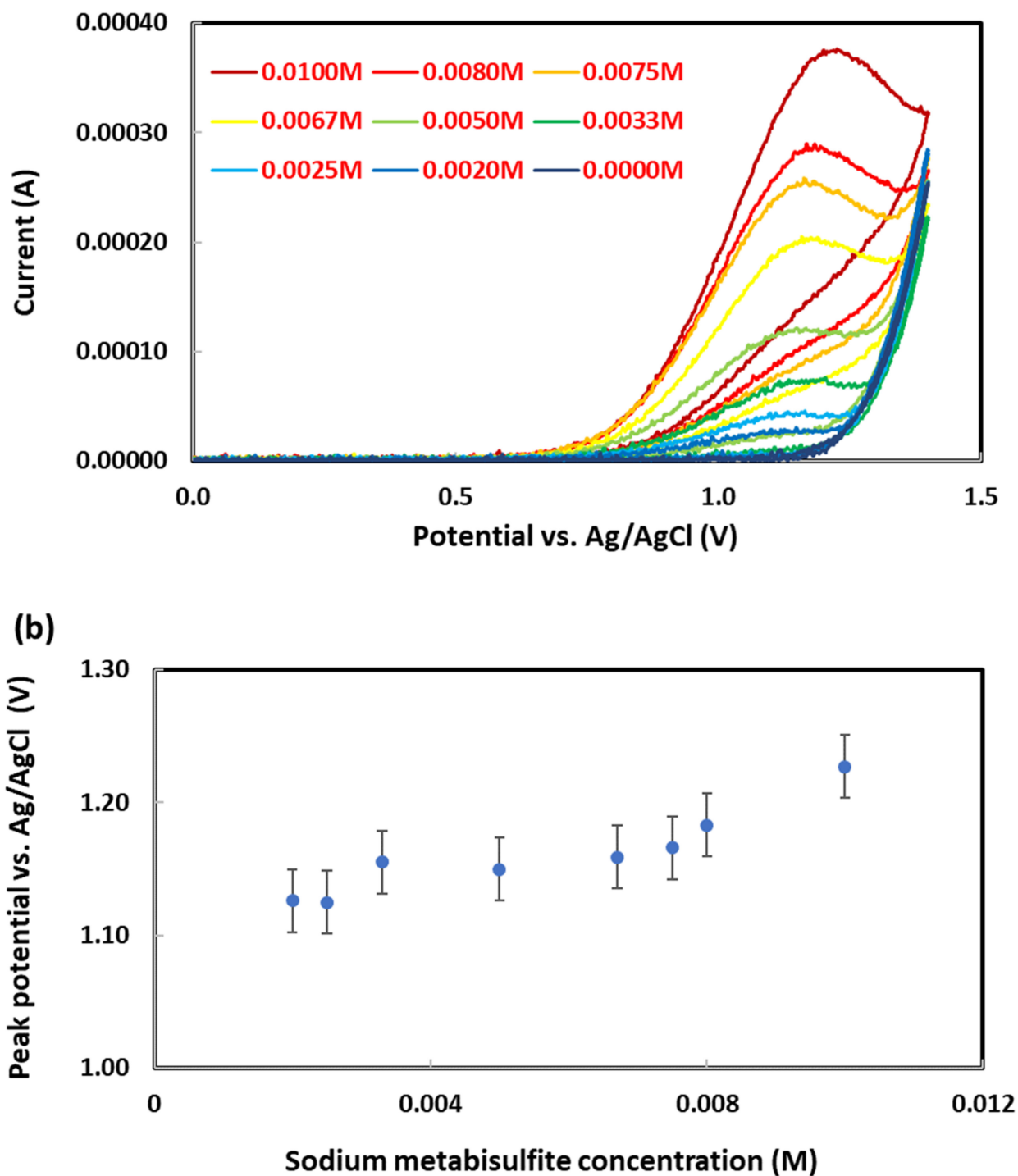


Figure 7. (a) Cyclic voltammograms of sodium metabisulfite at different concentrations on graphite electrodes deposited with 60 µg of ZnO nanoparticles. (b) Metasulfite oxidation peak potential vs. metabisulfite concentration tested.

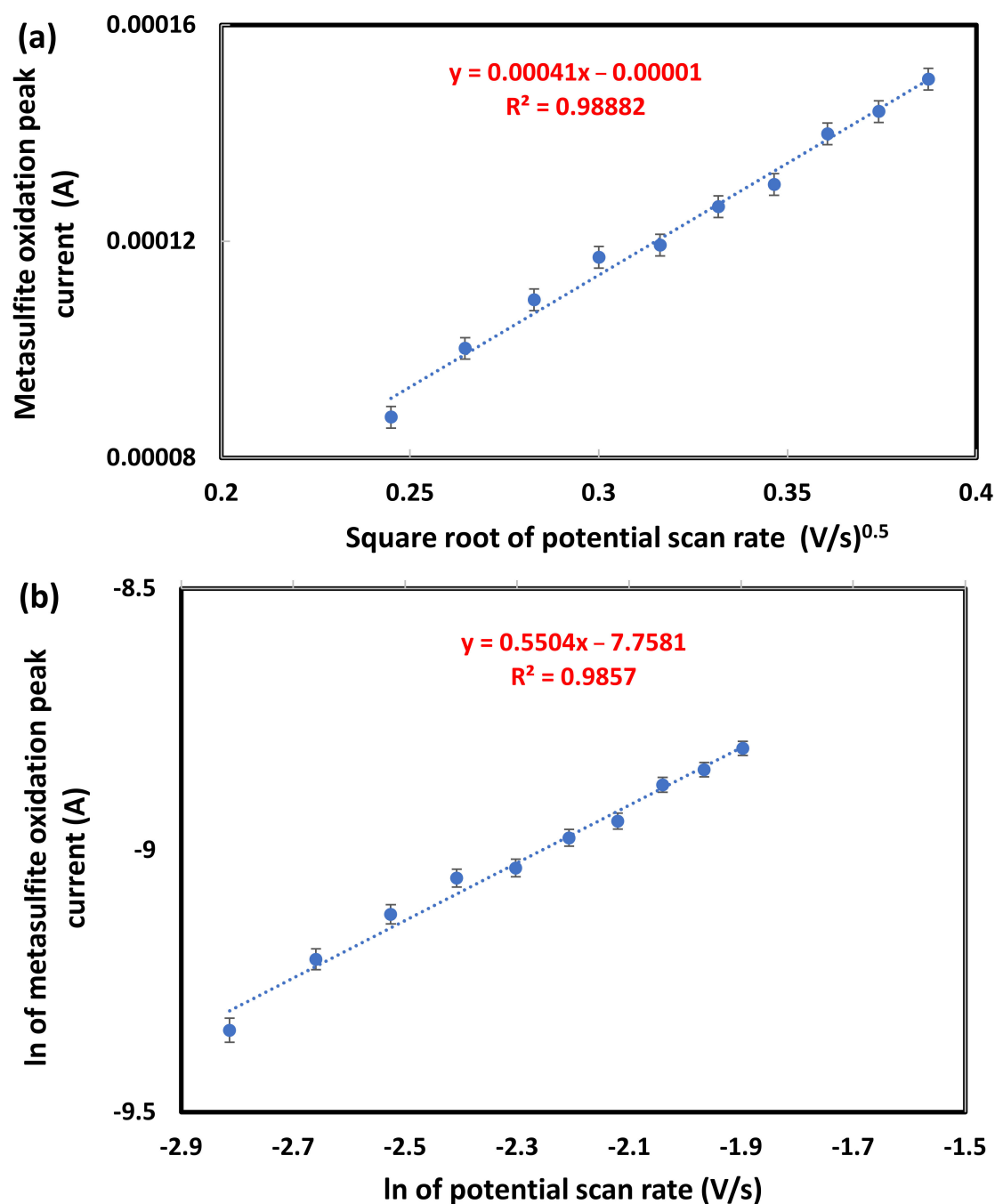


Figure 8. (a) Linear dependence of metasulfite oxidation peak current (I_{pa}) on square root of potential scan rate (v); (b) dependence of $\ln(I_{pa})$ on $\ln(v)$. Mass of ZnO nanoparticles deposited on SPE = 129 μg ; metabisulfite concentration in 1.0 M KCl for CV analysis = 0.003 M; potential scan rate = 0.006 to 0.15 V/s.

Chronoamperometric measurements of sodium metabisulfite at the graphite screen-printed electrode were carried out by setting the working electrode potential 1.40 V vs. Ag/AgCl for various concentrations as presented in Figure 9a. The metabisulfite oxidation current observed for the hydrolysis reaction ($\text{S}_2\text{O}_5^{2-} + \text{H}_2\text{O} \rightarrow 2\text{HSO}_3$) followed by electrochemical oxidation: $\text{HSO}_3^- + \text{H}_2\text{O} \rightarrow \text{SO}_4^{2-} + 2\text{e}^- + 3\text{H}^+$) under mass transport-limited conditions can be described by the Cottrell equation with a diffusion coefficient (D) [67]. Experimental plots of I vs. $t^{-1/2}$ were drawn, and the best straight-line fittings for different concentrations of metabisulfite were determined. The slopes of the resulting straight lines were then

plotted against metabisulfite concentrations in Figure 9b. From the resulting slope and the Cottrell equation, the value of D was found to be $4.16 \times 10^{-5} \text{ cm}^2 \text{ s}^{-1}$.

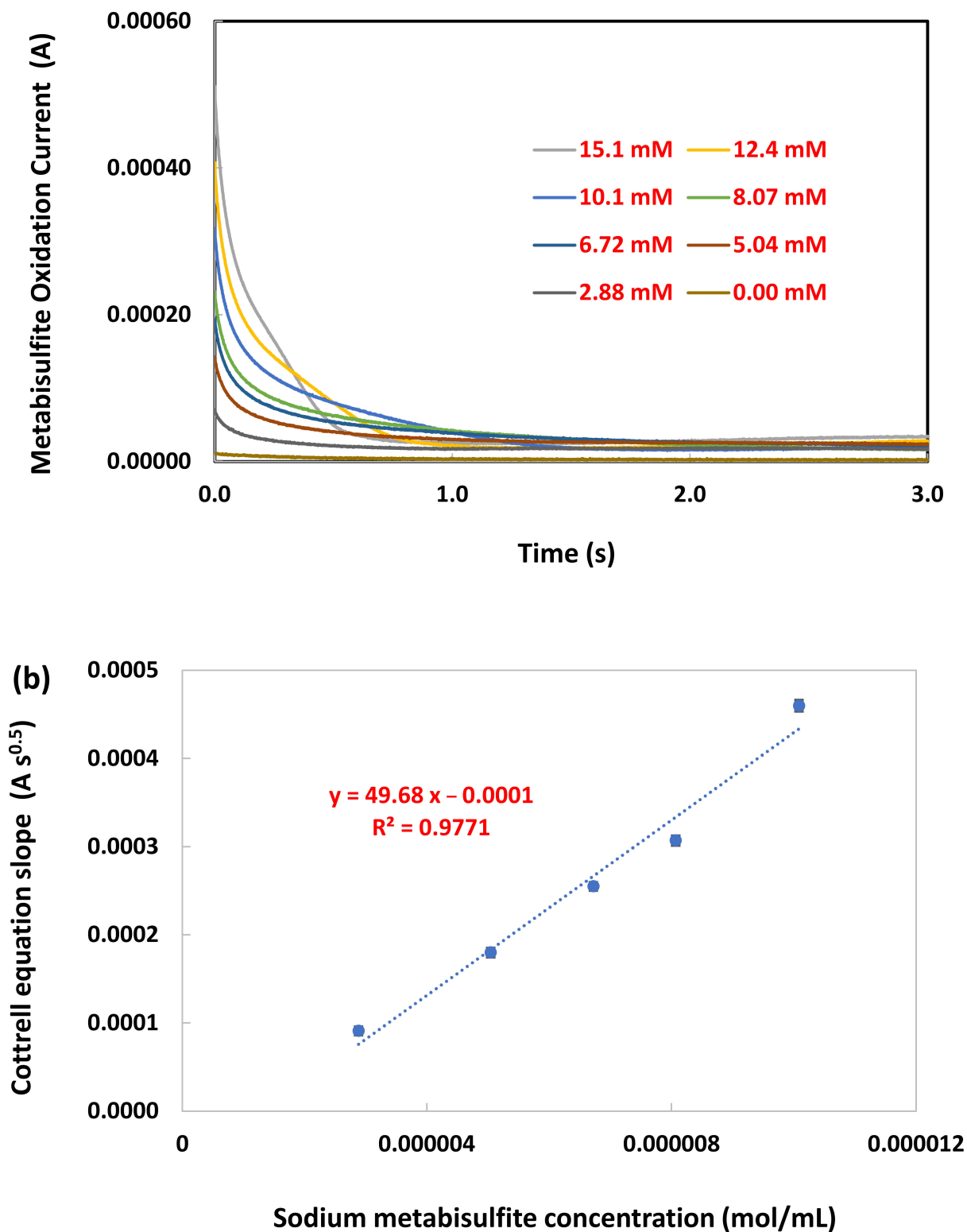


Figure 9. (a) Chronoamperograms obtained at graphite screen-printed electrode (0.3 cm diameter, deposited with 120 μg of ZnO nanoparticles) at 1.0 M KCl for different concentrations of sodium metabisulfite (from 0.00 to 12.1 mM). Applied potential = 1.40 V vs. Ag/AgCl reference electrode. (b) Plot of Cottrell equation slopes against sodium metabisulfite concentrations.

A further comparison was made by measuring the oxidation peak current of ascorbic acid (0.090 M in 1.0 M KCl) versus the mass of ZnO nanoparticles deposited on SPE. As shown in Figure S5, the ascorbic acid oxidation peak current did not vary significantly with increasing mass of ZnO nanoparticles deposited. Such a lack of dependency is in marked contrast to the metabisulfite peak current presented in Figure 5 above. This difference in electrochemical oxidation behavior between metabisulfite (a reducing agent) and ascorbic acid (an antioxidant) suggests that the oxidant activity of ZnO originates from the oxide anion (reactive towards reducing agents) rather than the superoxide anion or the hydroxyl radical (reactive towards antioxidants). In the scientific literature, some researchers called $\text{Na}_2\text{S}_2\text{O}_5$ an antioxidant and others called it a reducing agent. Here, we are clarifying it to be a reducing agent. This makes sense because $\text{Na}_2\text{S}_2\text{O}_5$ is a chemical that donates electrons, but not a biochemical that generates ROS as free radicals. Free radicals accept electrons donated by antioxidant, deactivate quickly, and convert to a less-active molecule by oxidation [68].

Next, 0.003 M L-glutathione in 1 M KCl solution was tested on SPEs deposited with various amounts of ZnO nanoparticles. As shown in Figure S6, although metabisulfite and glutathione have the same number of electrons transferred ($n = 2$), glutathione has actually a smaller oxidation current signal [69,70]. Similar to the trend presented for metabisulfite in Figure 5, the oxidation current increased nonlinearly until it reached a saturation level beyond 60 μg of ZnO. This similarity strongly suggests full coverage of the SPE by nanoparticles. Larger amounts of ZnO nanoparticles might just pile up on the first monolayer to increase its oxidation activity.

4. Conclusions

In this research, cyclic voltammetry was used to study the electrochemical oxidation of sodium metabisulfite by a deposit of ZnO nanoparticles on SPE. The metabisulfite oxidation peak currents increased with increasing mass of ZnO nanoparticles deposited. Based on the relationship between the metabisulfite oxidation peak current and the mass of ZnO nanoparticles deposited, quantitative electrochemical analysis of ZnO nanoparticles in aqueous suspension was demonstrated up to a deposition mass of 60 μg . Metabisulfite proved to be a promising redox probe to determine the concentration of ZnO nanoparticles suspended in water. Our study of metabisulfite oxidation current as a function of voltammetric scan rate indicated that the electrochemical process on the ZnO-deposited SPE was probably controlled by both adsorption and diffusion processes. No interference studies were conducted as the redox probe is selective toward ZnO nanoparticles due to the favorable interaction between Zn and S. The proposed method can be optimized in accordance with the target environmental study of interest to analyze various types of water. Future research and development of chemosensors for ZnO nanoparticles in our lab would evaluate other reducing agents that can attain a higher mass sensitivity for ZnO nanoparticles in aqueous suspension. Different electrode materials, supporting electrolytes, and pH levels can be evaluated to improve the sensing method for better detection limits.

Supplementary Materials: The following supporting information can be downloaded at: <https://www.mdpi.com/article/10.3390/chemosensors10040145/s1>, Figure S1: Cyclic voltammograms of ascorbic acid (0.003 M in 1.0 M KCl) on graphite electrode with ZnO nanoparticles in suspension (0.25 mg/mL) versus ZnO nanoparticles deposited on electrode (150 μL of 0.25 mg/mL). $E_{\text{initial}} = 0.0 \text{ V}$, $E_{\text{final}} = 1.4 \text{ V}$, scan rate = 0.10 V/s, scan direction = positive; Figure S2. Cyclic voltammograms of sodium metabisulfite (0.0057 M) for 0 μg and 115 μg of ZnO nanoparticles deposited on graphite electrode. $E_{\text{initial}} = 0.0 \text{ V}$, $E_{\text{final}} = 1.4 \text{ V}$, scan rate = 0.10 V/s, scan direction = positive; Figure S3. Cyclic voltammetric measurement results of potassium ferricyanide (0.006 M in 1.0 M KCl) oxidation peak current vs. mass of ZnO nanoparticles deposited on graphite electrode; Figure S4. Cyclic voltammetric measurement results of oxidation peak current vs. sodium metabisulfite concentration in 1.0 M KCl. Mass of ZnO nanoparticles deposited on graphite electrode = 60 μg or 115 μg ; Figure S5. Cyclic voltammetric measurement results of ascorbic acid (0.003 M in 1.0 M KCl) oxidation peak current vs. mass of ZnO nanoparticles deposited on graphite electrode; Figure S6. Cyclic

voltammetric measurement results of glutathione (0.003 M in 1.0 M KCl) oxidation peak current vs. mass of ZnO nanoparticles deposited on graphite electrode. Each data point represents the average current measured between 1.19 V and 1.21 V versus Ag/AgCl reference electrode.

Author Contributions: Conceptualization, E.P.C.L.; methodology, K.W. and E.P.C.L.; validation, E.P.C.L.; formal analysis, K.W.; resources, E.P.C.L.; writing—original draft preparation, K.W.; writing—review and editing, E.P.C.L.; supervision, E.P.C.L.; project administration, E.P.C.L.; funding acquisition, E.P.C.L. All authors have read and agreed to the published version of the manuscript.

Funding: Financial support from NSERC Canada (grant number RGPIN-2018-05320) is gratefully acknowledged.

Institutional Review Board Statement: Not applicable.

Informed Consent Statement: Not applicable.

Data Availability Statement: The authors confirm that the data supporting the findings of this study are available within the article and its supplementary materials. The raw data generated at Carleton University are available on request from the corresponding author.

Acknowledgments: The authors thank Meissam Noroozifar for helpful discussions and expert guidance.

Conflicts of Interest: The authors declare no conflict of interest.

References

1. Arunachalam, S.V.; Tammineni, V.S.; Espenti, C.S.; Mutyala, S. Chapter two—Metal oxide-modified electrochemical sensors for toxic chemicals. In *Metal Oxides in Nanocomposite-Based Electrochemical Sensors for Toxic Chemicals*; Elsevier: Amsterdam, The Netherlands, 2021; pp. 19–49.
2. Lee, D.Y.; Kang, S.; Lee, Y.; Kim, J.Y.; Yoo, D.; Jung, W.; Lee, S.; Jeong, Y.Y.; Lee, K.; Jon, S. PEGylated Bilirubin-coated Iron Oxide Nanoparticles as a Biosensor for Magnetic Relaxation Switching-based ROS Detection in Whole Blood. *Theranostics* **2020**, *10*, 1997–2007. [[CrossRef](#)] [[PubMed](#)]
3. Zeng, W.; Wang, L.; Shi, H.; Zhang, G.; Zhang, K.; Zhang, H.; Gong, F.; Wang, T.; Duan, H. Metal–organic-framework-derived ZnO@Co₂O₄ core–shell structures as an advanced electrode for high-performance supercapacitors. *J. Mater. Chem. Mater. Energy Sustain.* **2016**, *4*, 8233–8241. [[CrossRef](#)]
4. Saranya, M.; Ramachandran, R.; Wang, F. Graphene-zinc oxide (G-ZnO) nanocomposite for electrochemical supercapacitor applications. *J. Sci. Adv. Mater. Devices* **2016**, *1*, 454–460. [[CrossRef](#)]
5. Zhang, L.; Zhang, J.; Liu, Y.; Zhang, L.; Yuan, A. Porous ZnO/NiO Microspherical Structures Prepared by Thermolysis of Heterobimetallic Metal-Organic Framework as Supercapacitor Electrodes. *J. Nanosci. Nanotechnol.* **2017**, *17*, 2571–2577. [[CrossRef](#)]
6. Kalpana, V.N.; Rajeswari, V.D. A review on green synthesis, biomedical applications, and toxicity studies of ZnO nanoparticles. *Bioinorg. Chem. Appl.* **2018**, *2018*, 3569758. [[CrossRef](#)] [[PubMed](#)]
7. Raj, B.S.; Samraj, P.I. Zinc oxide nanoparticles: A biological and pharmaceutical review. *Nanosci. Nanotechnol. Asia* **2020**, *10*, e070820184647. [[CrossRef](#)]
8. Melnikova, N.; Vorobyova, O.; Balakireva, A.; Malygina, D.; Solovyeva, A.; Belyaeva, K.; Orekhov, D.; Knyazev, A. The new pharmaceutical compositions of zinc oxide nanoparticles and triterpenoids for the burn treatment. *Pharmaceuticals* **2020**, *13*, 207. [[CrossRef](#)]
9. Yadav, M.S.; Singh, N.; Kumar, A. Synthesis and characterization of zinc oxide nanoparticles and activated charcoal based nanocomposite for supercapacitor electrode application. *J. Mater. Sci. Mater. Electron.* **2018**, *29*, 6853–6869. [[CrossRef](#)]
10. Tashkhourian, J.; Hemmateenejad, B.; Beigizadeh, H.; Hosseini-Sarvari, M.; Razmi, Z. ZnO nanoparticles and multiwalled carbon nanotubes modified carbon paste electrode for determination of naproxen using electrochemical techniques. *J. Electroanal. Chem.* **2014**, *714–715*, 103–108. [[CrossRef](#)]
11. Umar, A.; Rahman, M.; Vaseem, M.; Hahn, Y.-B. Ultra-sensitive cholesterol biosensor based on low-temperature grown ZnO nanoparticles. *Electrochem. Commun.* **2009**, *11*, 118–121. [[CrossRef](#)]
12. Kegela, J.; Povey, I.M.; Pemble, M.E. Zinc oxide for solar water splitting: A brief review of the material’s challenges and associated opportunities. *Nano Energy* **2018**, *54*, 409–428. [[CrossRef](#)]
13. Kelly, S.R.; Shi, X.; Back, S.; Vallez, L.; Park, S.Y.; Siahrostami, S.; Zheng, X.; Nørskov, J.K. ZnO As an Active and Selective Catalyst for Electrochemical Water Oxidation to Hydrogen Peroxide. *ACS Catal.* **2019**, *9*, 4593–4599. [[CrossRef](#)]
14. Yuan, K.; Cao, Q.; Li, X.; Chen, H.Y.; Deng, Y.; Wang, Y.Y.; Luo, W.; Lu, H.L.; Zhang, D.W. Synthesis of WO₃@ZnWO₄@ZnO-ZnO hierarchical nanocactus arrays for efficient photoelectrochemical water splitting. *Nano Energy* **2017**, *41*, 543–551. [[CrossRef](#)]
15. Wang, L.; Yu, X.; Li, X.; Zhang, J.; Wang, M.; Che, R. MOF-derived yolk-shell Ni@C@ZnO Schottky contact structure for enhanced microwave absorption. *Chem. Eng. J.* **2020**, *383*, 123099. [[CrossRef](#)]

16. Ancona, A.; Dumontel, B.; Garino, N.; Demarco, B.; Chatzitheodoridou, D.; Fazzini, W.; Engelke, H.; Cauda, V. Lipid-Coated Zinc Oxide Nanoparticles as Innovative ROS-Generators for Photodynamic Therapy in Cancer Cells. *Nanomaterials* **2018**, *8*, 143. [[CrossRef](#)] [[PubMed](#)]
17. Sirelkhatim, A.; Mahmud, S.; Seeni, A.; Kaus, N.H.M.; Ann, L.C.; Bakhori, S.K.M.; Hasan, H.; Mohamad, D. Review on Zinc Oxide Nanoparticles: Antibacterial Activity and Toxicity Mechanism. *Nano-Micro Lett.* **2015**, *7*, 219–242. [[CrossRef](#)] [[PubMed](#)]
18. Jorne, J.; Gillespie, M.; Chen, D.; Zhou, D. Nano-electrochemical of fluidized particles: Solid state reduction of ZnO nano-particles. *J. Electrochem. Soc.* **2013**, *160*, H203. [[CrossRef](#)]
19. Alamdari, S.; Ghamsari, M.S.; Lee, C.; Han, W.; Park, H.-H.; Tafreshi, M.J.; Afarideh, H.; Ara, M.H.M. Preparation and Characterization of Zinc Oxide Nanoparticles Using Leaf Extract of *Sambucus ebulus*. *Appl. Sci.* **2020**, *10*, 3620. [[CrossRef](#)]
20. Selim, Y.A.; Azb, M.A.; Ragab, I.; Abd El-Azim, M.H.M. Green Synthesis of Zinc Oxide Nanoparticles Using Aqueous Extract of *Deverra tortuosa* and their Cytotoxic Activities. *Sci. Rep.* **2020**, *10*, 3445. [[CrossRef](#)]
21. Yusof, H.M.; Mohamad, R.; Zaidan, U.H.; Rahman, N.A. Sustainable microbial cell nanofactory for zinc oxide nanoparticles production by zinc-tolerant probiotic *Lactobacillus plantarum* strain TA4. *Microb. Cell Factories* **2020**, *19*, 10. [[CrossRef](#)]
22. Safawo, T.; Sandeep, B.V.; Pola, S.; Tadesse, A. Synthesis and characterization of zinc oxide nanoparticles using tuber extract of anchote for antimicrobial and oxidant activity assessment. *OpenNano* **2018**, *3*, 56–63. [[CrossRef](#)]
23. Navale, G.R.; Thripuranthaka, M.; Late, D.J.; Shinde, S.S. Antimicrobial activity of ZnO nanoparticles against pathogenic bacteria and fungi. *JSM Nanotechnol. Nanomed.* **2015**, *3*, 1033.
24. Yu, K.-N.; Yoon, T.-J.; Minai-Tehrani, A.; Kim, J.-E.; Park, S.J.; Jeong, M.S.; Ha, S.-W.; Lee, J.-K.; Kim, J.S.; Cho, M.-H. Zinc oxide nanoparticle induced autophagic cell death and mitochondrial damage via reactive oxygen species generation. *Toxicol. Vitro.* **2013**, *27*, 1187–1195. [[CrossRef](#)] [[PubMed](#)]
25. Kaya, H.; Aydın, F.; Gürkan, M.; Yılmaz, S.; Ates, M.; Demir, V.; Arslan, Z. A comparative toxicity study between small and large size zinc oxide nanoparticles in tilapia (*Oreochromis niloticus*): Organ pathologies, osmoregulatory responses and immunological parameters. *Chemosphere* **2016**, *144*, 571–582. [[CrossRef](#)]
26. Samei, M.; Sarrafzadeh, M.-H.; Faramarzi, M.A. The impact of morphology and size of zinc oxide nanoparticles on its toxicity to the freshwater microalga, *Raphidocelis subcapitata*. *Environ. Sci. Pollut. Res.* **2018**, *26*, 2409–2420. [[CrossRef](#)]
27. Singh, T.A.; Das, J.; Sil, P.C. Zinc oxide nanoparticles: A comprehensive review on its synthesis, anticancer and drug delivery applications as well as health risks. *Adv. Colloid Interface Sci.* **2020**, *286*, 102317. [[CrossRef](#)]
28. Li, L.; Fernandez-Cruz, M.L.; Connolly, M.; Conde, E.; Fernández, M.; Schuster, M.; Navas, J.M. The potentiation effect makes the difference: Non-toxic concentrations of ZnO nanoparticles enhance Cu nanoparticle toxicity in vitro. *Sci. Total Environ.* **2015**, *505*, 253–260. [[CrossRef](#)]
29. Vinardell, M.P.; Mitjans, M. Antitumor Activities of Metal Oxide Nanoparticles. *Nanomaterials* **2015**, *5*, 1004–1021. [[CrossRef](#)]
30. Dimapilis, E.A.S.; Hsu, C.-S.; Mendoza, R.M.O.; Lu, M.-C. Zinc oxide nanoparticles for water disinfection. *Sustain. Environ. Res.* **2018**, *28*, 47–56. [[CrossRef](#)]
31. Fréchette-Viens, L.; Hadioui, M.; Wilkinson, K.J. Quantification of ZnO nanoparticles and other Zn containing colloids in natural waters using a high sensitivity single particle ICP-MS. *Talanta* **2019**, *200*, 156–162. [[CrossRef](#)]
32. Yang, Y.; Liu, X.; Luo, L.; Wei, W.; Wang, Q.; Zhang, J. Quantitative Detection of Zinc Oxide Nanoparticle in Environmental Water by Cloud Point Extraction Combined ICP-MS. *Adsorpt. Sci. Technol.* **2021**, *2021*, 1–10. [[CrossRef](#)]
33. Sonage, B.; Mohanan, P. Characterization of Zinc Oxide Nanoparticles used for Preparation of Nanofluids. *Procedia Mater. Sci.* **2014**, *5*, 1160–1164. [[CrossRef](#)]
34. Mahamuni, P.P.; Patil, P.M.; Dhanavade, M.J.; Badiger, M.V.; Shadija, P.G.; Lokhande, A.C.; Bohara, R.A. Synthesis and characterization of zinc oxide nanoparticles by using polyol chemistry for their antimicrobial and antibiofilm activity. *Biochem. Biophys. Rep.* **2019**, *17*, 71–80. [[CrossRef](#)] [[PubMed](#)]
35. Benekohal, N.P.; Demopoulos, G.P. Electrophoretically self-assembled mixed metal oxide-TiO₂ nano-composite film structures for photoelectrochemical energy conversion: Probing of charge recombination and electron transport resistances. *J. Power Sources* **2013**, *240*, 667–675. [[CrossRef](#)]
36. Wang, K.; Zhang, W.; Lai, E.P.C. Electrochemical Impedance Spectroscopy of Zinc Oxide Nanoparticles After Deposition on Screen Printed Electrode. *J. Nanosci. Nanotechnol.* **2021**, *21*, 5207–5214. [[CrossRef](#)] [[PubMed](#)]
37. Ravikumar, C.; Kotteeswaran, P.; Murugan, A.; Raju, V.B.; Santosh, M.; Nagaswarupa, H.; Nagabhushana, H.; Prashantha, S.; Kumar, M.A.; Gurushantha, K. Electrochemical Studies of Nano Metal Oxide Reinforced Nickel Hydroxide Materials for Energy Storage Applications. *Mater. Today Proc.* **2017**, *4*, 12205–12214. [[CrossRef](#)]
38. Najim, N.; Rusdi, R.; Hamzah, A.S.; Shaameri, Z.; Zain, M.M.; Kamarulzaman, N. Effects of the Absorption Behaviour of ZnO Nanoparticles on Cytotoxicity Measurements. *J. Nanomater.* **2014**, *2014*, 1–10. [[CrossRef](#)]
39. Zhao, Y.; Wang, M. Experimental study on dielectric relaxation of SiO₂ nano-particle suspensions for developing a particle characterization method based on electrical impedance spectroscopy. *Powder Technol.* **2015**, *281*, 200–213. [[CrossRef](#)]
40. Oliveira, C.M.; Barros, A.S.; Ferreira, A.C.; Silva, A.M. Study of quinones reactions with wine nucleophiles by cyclic voltammetry. *Food Chem.* **2016**, *211*, 1–7. [[CrossRef](#)]
41. Wang, H.-W.; Bringans, C.; Hickey, A.; Windsor, J.; Kilmartin, P.; Phillips, A. Cyclic Voltammetry in Biological Samples: A Systematic Review of Methods and Techniques Applicable to Clinical Settings. *Signals* **2021**, *2*, 138–158. [[CrossRef](#)]

42. Apak, R.; Özyürek, M.; Güçlü, K.; Çapanoğlu, E. Antioxidant Activity/Capacity Measurement. 1. Classification, Physicochemical Principles, Mechanisms, and Electron Transfer (ET)-Based Assays. *J. Agric. Food Chem.* **2016**, *64*, 997–1027. [CrossRef] [PubMed]
43. Shabliyy, T.; Gomelya, M.; Pohrebennyk, V.; Ivanenko, O.; Nosachova, Y. Development of New Water Deoxidization Systems for Heat and Power Plants. *J. Ecol. Eng.* **2022**, *23*, 193–205. [CrossRef]
44. Larmené-Beld, K.H.M.; Van Berkel, S.; Wijnsma, R.; Taxis, K.; Frijlink, H.W. Prefilled Cyclic Olefin Sterilized Syringes of Norepinephrine Injection Solution Do Not Need to Be Stabilized by Antioxidants. *AAPS PharmSciTech* **2020**, *21*, 247. [CrossRef] [PubMed]
45. National Center for Biotechnology Information. Sodium Metabisulfite. Available online: <https://pubchem.ncbi.nlm.nih.gov/compound/Sodium-metabisulfite> (accessed on 12 October 2021).
46. Ratanajanchai, M.; Kanchanasavita, W.; Suputtamongkol, K.; Wonglamsam, A.; Thamapipol, S.; Sae-Khow, O. Heat-cured poly(methyl methacrylate) resin incorporated with different food preservatives as an anti-microbial denture base material. *J. Dent. Sci.* **2021**, *16*, 706–712. [CrossRef]
47. Cosmetics Info. Sodium Metabisulfite. Available online: <https://www.cosmeticsinfo.org/ingredients/sodium-metabisulfite/> (accessed on 2 April 2022).
48. Campbell, J.R.; Maestrello, C.L.; Campbell, R.L. Allergic response to metabisulfite in lidocaine anesthetic solution. *Anesth. Prog.* **2001**, *48*, 21–26.
49. Bakerpedia. Sodium Metabisulfite. Available online: <https://bakerpedia.com/ingredients/sodium-metabisulfite/> (accessed on 12 October 2021).
50. American Water Chemicals. Is Sodium Metabisulfite an Effective Disinfectant for My RO System? Available online: <https://www.membranechemicals.com/faqs/sodium-metabisulfite-effective-disinfectant-ro-system/> (accessed on 12 October 2021).
51. Jeong, S.; Lee, H.; Cho, C.H.; Yoo, S. Characterization of multi-functional, biodegradable sodium metabisulfite-incorporated films based on polycaprolactone for active food packaging application. *Anal. Methods* **2020**, *25*, 100512.
52. Zaid, B.; Maddache, N.; Saidi, D.; Souami, N.; Bacha, N.; Ahmed, A.S. Electrochemical evaluation of sodium metabisulfite as environmentally friendly inhibitor for corrosion of aluminum alloy 6061 in a chloride solution. *J. Alloys Compd.* **2015**, *629*, 188–196. [CrossRef]
53. Quintino, M.S.; Araki, K.; Toma, H.E.; Angnes, L. Amperometric quantification of sodium metabisulfite in pharmaceutical formulations utilizing tetraruthenated porphyrin film modified electrodes and batch injection analysis. *Talanta* **2006**, *68*, 1281–1286. [CrossRef]
54. Gil, D.M.D.A.; Rebelo, M.J.F. Metabisulfite interference in biosensing and Folin-Ciocalteu analysis of polyphenols. *Microchim. Acta* **2009**, *167*, 253–258. [CrossRef]
55. Durairaj, S.; Manikandan, V.; Dingle, S.; Wang, Q.; Chen, A. Nanomaterial-Based Electrochemical Sensor for the Detection of Sodium Metabisulfite in Stimulated Digestive Fluids. Available online: <https://www.uoguelph.ca/foodscience/system/files/Durairaj%20-%20poster%20abstract%20GFSS%20symposium%202019.pdf> (accessed on 28 March 2022).
56. Pare, A.; Ghosh, S.K. Temperature Dependent Rheological Behavior of Zinc Oxide Based Water Nanofluid. In *Proceedings of the 25th National and 3rd International ISHMT-ASTFE Heat and Mass Transfer Conference (IHMT-2019)*; Begell House Inc.: Danbury, CT, USA, 2019; pp. 317–321.
57. Moumene, M.; Rochefort, D.; Mohamedi, M. Electrochemical functionalization as a promising avenue for glucose oxidase immobilization at carbon nanotubes: Enhanced direct electron transfer process. *Int. J. Electrochem. Sci.* **2013**, *8*, 2009–2022.
58. Krishnamoorthy, K.; Ananth, A.; Mok, Y.S.; Kim, S.-J. Plasma Assisted Synthesis of Graphene Nanosheets and Their Supercapacitor Applications. *Sci. Adv. Mater.* **2014**, *6*, 349–353. [CrossRef]
59. Zhou, D.; Keller, A.A. Role of morphology in the aggregation kinetics of ZnO nanoparticles. *Water Res.* **2010**, *44*, 2948–2956. [CrossRef] [PubMed]
60. Rao, V.R. Chapter 7—Antioxidant agents. In *Advances in Structure and Activity Relationship of Coumarin Derivatives*; Penta, S., Ed.; Elsevier: Amsterdam, The Netherlands, 2016; pp. 137–150.
61. Zhang, W.; Lai, E.P. Electrochemical detection of zinc oxide nanoparticles in water contamination analysis based on surface catalytic reactivity. *J. Nanopart. Res.* **2020**, *22*, 95. [CrossRef]
62. Al-Mohaimeed, A.; Al-Onazi, W.A.; El-Tohamy, M. Utility of Zinc Oxide Nanoparticles Catalytic Activity in the Electrochemical Determination of Minocycline Hydrochloride. *Polymers* **2020**, *12*, 2505. [CrossRef] [PubMed]
63. Rupasinghe, R.A.T.P. Dissolution and Aggregation of zinc Oxide Nanoparticles at Circumneutral pH: A Study of Size Effects in the Presence and Absence of Citric Acid. Master's Thesis, University of Iowa, Iowa City, IA, USA, 2011.
64. Castelli, I.E.; Thygesen, K.S.; Jacobsen, K.W. Calculated Pourbaix Diagrams of Cubic Perovskites for Water Splitting: Stability Against Corrosion. *Top. Catal.* **2014**, *57*, 265–272. [CrossRef]
65. Gómez-Gil, J.M.; Laborda, E.; Molina, A. General Explicit Mathematical Solution for the Voltammetry of Nonunity Stoichiometry Electrode Reactions: Diagnosis Criteria in Cyclic Voltammetry. *Anal. Chem.* **2020**, *92*, 3728–3734. [CrossRef]
66. LibreTexts. Important Parameters in CV. Available online: [https://chem.libretexts.org/Bookshelves/Analytical_Chemistry/Supplemental_Modules_\(Analytical_Chemistry\)/Analytical_Sciences_Digital_Library/JASDL/Courseware/Analytical_Electrochemistry%3A_The_Basic_Concepts/04_Voltammetric_Methods/A._Basics_of_Voltammetry/02_Potential_Sweep_Methods/b\)_Cyclic_Voltammetry/ii\)_Important_parameters_in_CV](https://chem.libretexts.org/Bookshelves/Analytical_Chemistry/Supplemental_Modules_(Analytical_Chemistry)/Analytical_Sciences_Digital_Library/JASDL/Courseware/Analytical_Electrochemistry%3A_The_Basic_Concepts/04_Voltammetric_Methods/A._Basics_of_Voltammetry/02_Potential_Sweep_Methods/b)_Cyclic_Voltammetry/ii)_Important_parameters_in_CV) (accessed on 12 October 2021).

67. Rajabi, H.; Noroozifar, M.; Khorasani-Motlagh, M. Graphite paste electrode modified with Lewatit® FO36 nano-resin for simultaneous determination of ascorbic acid, acetaminophen and tryptophan. *Anal. Methods* **2016**, *8*, 1924–1934. [[CrossRef](#)]
68. Lobo, V.; Patil, A.; Phatak, A.; Chandra, N. Free radicals, antioxidants and functional foods: Impact on human health. *Pharmacogn. Rev.* **2010**, *4*, 118–126. [[CrossRef](#)]
69. Hunger, T.; Lopicque, F. Electrochemistry of the oxidation of sulfite and bisulfite ions at a graphite surface: An overall approach. *Electrochim. Acta* **1991**, *36*, 1073–1082. [[CrossRef](#)]
70. Saranya, S.; Jency, F.J.; Geetha, B.; Deepa, P.N. Simultaneous detection of glutathione, threonine, and glycine at electrodeposited RuHCH/rGO-modified electrode. *Ionics* **2019**, *25*, 5537–5550. [[CrossRef](#)]